Geological Quarterly, 2026, 70, 18
DOI: https://doi.org/10.7306/gq.1863

Integrated mineralogical and colour analysis of the Poznań Clays from the Honoratka dump near Konin in Central Poland

Jakub KLĘSK[1, *], Łukasz KRUSZEWSKI[2], Artur BŁACHOWSKI[3] and Marek WIDERA[1]

[1] Institute of Geology, Adam Mickiewicz University, Krygowskiego 12, 61–680 Poznań, Poland ORCID: 0000–0001–7437–1232 [J.K.], 0000-0001-5092-2845 [M.W.]

[2] Institute of Geological Sciences, Polish Academy of Sciences, Twarda 51/55, 00-818 Warszawa, Poland, ORCID: 0000-0001-6332-9944 [Ł.K.]

[3] AGH University of Krakow, Faculty of Geology, Geophysics and Environmental Protection, al. Mickiewicza 30, 30-059 Kraków, Poland, ORCID: 0000-0002-5591-5756 [A.B.]

Klęsk, J., Kruszewski, Ł., Błachowski, A., Widera, M., 2026. Integrated mineralogical and colour analysis of the Poznań Clays from the Honoratka dump near Konin in central Poland. Geological Quarterly, **70**: 18; https://doi.org/10.7306/gq.1863

The Poznań Clays represent a key lithostratigraphic unit of the Neogene in the Polish Lowlands. They are characterised by pronounced colour variability, ranging from dark grey and black to yellow, brown and red. This study identifies and quantifies the mineralogical and geochemical factors controlling this colour variability and evaluates their significance for palaeoenvironmental interpretation, using samples collected from the Honoratka dump in central Poland. A multimethod approach is applied, including grain-size analysis, Powder X-ray Diffraction (PXRD), ^{57}Fe Mössbauer Spectroscopy (^{57}Fe-MS), Scanning Electron Microscopy with Energy-Dispersive X-ray Spectroscopy (SEM-EDS), and Raman Spectroscopy (RS). The results obtained demonstrate that colour in the Poznań Clays is primarily controlled by the type, distribution, and crystallinity of iron-bearing phases, particularly hematite, goethite and jarosite, as well as by redox conditions, pH, and the presence of organic matter. Red and brown colours are associated with oxidising environments and the formation of hematite and goethite, while dark colours reflect reducing conditions and organic-matter preservation. Pale colours are linked to the dominance of non-pigmenting minerals such as quartz, clay minerals and carbonates. This study corroborates the effective use of sediment colour as an integrated indicator of depositional and post-depositional processes in palaeoenvironmental interpretations, when supported by mineralogical analyses.

Key words: sediment colour, sediment mineralogy, iron-oxide pigmentation, redox conditions, upper Neogene palaeogeography, Polish Lowlands.

INTRODUCTION

The Poznań Clays are a significant Neogene lithostratigraphic unit in the Polish Lowlands. Their presence and characteristics play a pivotal role in palaeoenvironmental reconstructions, as well as stratigraphic and palaeogeographic interpretations (e.g., Areń, 1964; Ciuk and Pożaryska, 1982; Badura and Przybylski, 2004; Widera, 2013). The Poznań Clays are of great significance as an archive of climatic and sedimentary changes in the late Neogene, as repeatedly emphasised in the literature (e.g., Bojakowska et al., 2010; Kasiński and Słodkowska, 2016; Kędzior et al., 2021; Widera et al., 2019, 2021a, b).

Of particular interest is the lithological and mineralogical diversity of these clayey deposits. This is reflected in their colour, ranging from black, shades of grey and green, to brown and red (Ciuk, 1970; Dyjor, 1970; McBride, 1974; Bown and Kraus, 1981, 1987; Choma-Moryl, 1988; Środoń et al., 2001; Cornell and Schwertmann, 2003; Christiansen, 2004; Duczmal-Czernikiewicz, 2010, 2013; Środoń et al., 2014; Colombo et al., 2016; Card and Montenari, 2023; Widera and Klęsk, 2025). The colour of the clays is a macroscopic feature that is easily visible in the field but its interpretive potential has been limited to date. Clay colour is determined by the presence of specific clay minerals (muscovite, smectite, kaolinite, and chlorite), with iron-bearing phases (hematite, goethite or siderite) playing a particularly significant role. The colour shades, ranging from greenish to reddish, are attributed to the proportions of these minerals and their oxidation state (Bown and Kraus, 1981, 1987; Duczmal-Czernikiewicz, 2013). In many studies, colour has been simply used descriptively. However, it can serve as a sensitive indicator of diagenetic processes, including the degree of oxidation of the sedimentary environment and subsequent mineral transformations (e.g., Górniak et al., 2001; Dyar et al., 2006; Górnicki et al., 2007; Hartemink, 2009; Habashi, 2016; Goldstein et al., 2017; Jiang et al., 2022; Johnson, 2014; Klęsk, 2023).

* Corresponding author, e-mail: jakub.klesk@amu.edu.pl

Received: May 31, 2026; accepted: July 2, 2026; first published online: July 24, 2026

Modern instrumental methods allow precise correlation between sediment colour and the mineralogy, grain-size distribution and microstructure of the Poznań Clays. Powder X-ray diffraction (PXRD) provides quantitative constraints on the bulk clay content and clay-mineral composition, which in this study are directly compared with objectively measured colour parameters rather than with descriptive colour classes alone (Kraus, 1999; Klęsk et al., 2022, 2023). ^{57}Fe Mössbauer spectroscopy (^{57}Fe-MS) is used here not only to confirm the presence of the main Fe-bearing pigments identified previously – hematite, goethite and jarosite – but also to quantify their relative proportions and Fe oxidation states across differently coloured levels of the Poznań Clays (Bąk et al., 2020; Lempart-Drozd et al., 2022; Makiel et al., 2022). Scanning electron microscopy with energy-dispersive X-ray spectroscopy (SEM-EDS) enables microstructural and chemical analysis (Kruszewski, 2013). Raman spectroscopy (RS) further constrains the identification of individual Fe-bearing phases at the microscale and helps to distinguish poorly crystalline goethite and jarosite from nano-hematite within pigment aggregates (Trąbska, 2015). This is further supported by grain-size analysis, which facilitates assessment of the role of grain fractions in shaping the optical properties of clays (Bown and Kraus, 1981; Kraus and Aslan, 1993; Duczmal-Czernikiewicz, 2013; Mancini et al., 2020). In combination, these methods provide a novel, fully quantitative framework for explaining the colour variability of the Poznań Clays in terms of mineralogical speciation, Fe redox state and pigment microtextures, thereby extending our earlier, more descriptive studies of Fe-bearing colouring minerals in these deposits.

This research was conducted on material from the Honoratka dump (Fig. 1), which is an anthropogenic mineral deposit (Widera and Szczurek, 2014). This dump is formed of Poznań Clays excavated and moved during lignite mining. This means that the clayey deposits examined have also been weathered in recent years.

Nevertheless, the major goal of this study is to demonstrate that their colours can be utilised as a comprehensive interpretative tool and not only as a descriptive, textural feature. The application of a number of the analytical techniques (PXRD, ^{57}Fe-MS, SEM-EDS, RS, etc.) noted above allowed for the comparison of sedimentary colour with mineral composition and microstructure. The research results described below can be compared with those for the Poznań Clays and other deposits elsewhere in the Polish Lowlands (Klęsk et al., 2022, 2023; Klęsk, 2023).

STUDY OBJECT AND GEOLOGICAL SETTING

FORMATION OF THE HONORATKA DUMP

In the Konin region, the investigation of the Poznań Clays, accompanying lignite-rich deposits, commenced as early as the late 1950s. Research conducted by Kuhl (1958) and Mazur (1959) demonstrated their potential for ceramic production. The estimated resources, at that time, amounted to 82 million m^3. Then, a decision was made to collect the Poznań Clays in special dumps (so-called 'anthropogenic mineral deposits'), located near to opencast lignite mines. One such site is the Honoratka dump (Fig. 1), which was created in 1988–1991 at the Pątnów opencast mine, close to a newly constructed brickyard in the village of Honoratka, which was put into operation in 1991. Ultimately, over 1.3 million m^3 of the Poznań Clays were deposited in this dump (Widera and Szczurek, 2014).

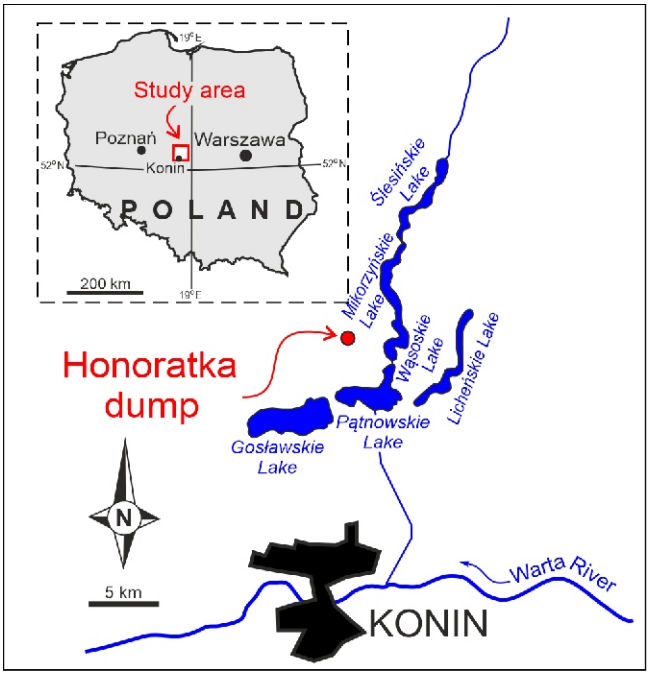

Fig. 1. The Honoratka dump studied relative to the town of Konin in Central Poland

GEOLOGICAL SETTING

The Pątnów opencast lignite mine, located west of the Honoratka dump (Fig. 1), contains a complete Neogene stratigraphic profile, overlain by Quaternary deposits. Lithostratigraphically, the Neogene is locally divided into two primary units, the Koźmin Formation below and the Poznań Formation above. The Koźmin Formation is composed of fluvial sands and carbonaceous sand with relatively thin lignite layers, that constitute the underburden of the first Mid-Polish lignite deposit (MPLS-1; e.g., Widera, 2007, 2021; Widera et al., 2023).

The Poznań Formation was subdivided into two lithostratigraphic members by Piwocki and Ziembińska-Tworzydło (1997). The lower member is the Grey Clay Member, which is predominantly composed of MPLS-1 in the Pątnów opencast mine, while the rest are 'grey clays'. The Wielkopolska Member, resting at the top of MPLS-1 and/or the 'grey clays', comprises over 95 vol.% of the multicoloured fine-grained deposits (i.e. 'green clays' and 'flamy clays'), which constitute the dominant part of the Poznań Clays (Piwocki and Ziembińska-Tworzydło, 1997; Widera, 2007, 2013; Widera et al., 2017, 2019; Zieliński and Widera, 2020). The deposits described, from which the samples H1–H8 were taken for laboratory analyses (Fig. 2), accumulated in the period ~13.8–5.0 Ma, i.e. from the latest Middle Miocene to the earliest Early Pliocene (Troć and Sadowska, 2006; Widera et al., 2021a, b; Widera and Klęsk, 2025).

LABORATORY RESEARCH METHODS

GRAIN-SIZE ANALYSIS AND ORGANIC MATTER DETERMINATION

The grain size of the samples was determined by laser diffraction (using a *Malvern Mastersizer 2000* analyser). The results of the grain-size analysis are shown as volume fractions of clay (<2 μm), silt (2–63 μm) and sand (>63 μm). The mean grain

Fig. 2. Multicoloured and powdered samples from the Honoratka dump examined mineralogically in this study

H1 – black, H2 – grey, H3 – yellow-brown, H4 – yellow, H5 – red, H6 – dark red, H7 – brownish-grey, H8 – light grey

size was calculated using the *GRADISTAT 5.11* program (Blott and Pye, 2001), which is widely used for the statistical treatment of unconsolidated sediments in fluvial and lacustrine settings. The sedimentary classification was conducted in accordance with two distinct schemes. The U.S. Department of Agriculture (USDA; Soil Survey Staff, 1951) scheme is primarily utilised in the context of soil studies, while Shepard's scheme (Shepard, 1954) is frequently employed in sedimentology and engineering geology. The grain-size analysis was performed by the Department of Geomorphology at the Adam Mickiewicz University in Poznań, Poland.

The presence of organic matter in the samples was confirmed by subjecting them to a treatment with hot 30% H_2O_2 solution. This was conducted at the Institute of Geology, Adam Mickiewicz University in Poznań.

POWDER X-RAY DIFFRACTION (PXRD)

Powder X-ray diffraction (PXRD) was used to analyse the mineral composition of eight samples (H1–H8) which show different colours. The samples were pulverised into a fine powder and analysed using a Bruker D8 Advance diffractometer operating in Bragg-Brentano – mode with a 260 mm goniometer radius. The diffractometer was configured with a Johansson monochromator that utilised Cu K 1 radiation (= 1.5406Å) and a LynxEye strip detector. The parameters for the current were 40 kV, 30 mA, and 1200 W. The scan range was configured from 2° to 35° 2 in continuous scanning mode. The scanning velocity was 0.6°/min, the measurement duration was 2 s and the step size was 0.02° 2 . To ensure a more random distribution of grain orientations relative to the X-ray beam, the samples were rotated during the measurement.

The results from the bulk samples were analysed using *Profex 5.5.2* software. *Profex Rietveld Refinement* software was used to determine the quantitative mineral content present in each sample by employing the Rietveld method (Rietveld, 1969; Mindat, 2022). For the purposes of this study, samples were collected and then processed into composite samples, in accordance with the material preparation procedures described by Kruszewski (2013) and Klęsk et al. (2022), among others. In order to determine the mineral composition of samples H1–H8, qualitative PXRD analysis and quantitative analysis were performed, which allowed for the identification of the dominant phases and the estimation of their percentage shares. The results obtained formed the basis for a comparative analysis of the mineral composition of the samples analysed. The PXRD measurements were carried out at the Environmental Laboratory for Unique Chemical Instrumentation, which belongs to the Faculty of Chemistry, Adam Mickiewicz University in Poznań.

^{57}Fe MÖSSBAUER SPECTROSCOPY (^{57}Fe-MS)

The ^{57}Fe-MS measurements were performed at room temperature in transmission geometry, by applying a RENON MsAa-4 spectrometer (Górnicki et al., 2007; Błachowski et al., 2008) equipped with an LND Kr-filled proportional detector and ^{57}Co(Rh) source. The absorbers for Mössbauer measurements were prepared using 40 mg/cm^2 of the materials investigated. The spectra obtained were fitted using the *MOSGRAF* data processing software suite. The ^{57}Fe-MS measurements were performed at the Faculty of Geology, Geophysics and Environmental Protection, AGH University in Kraków.

SCANNING ELECTRON MICROSCOPY WITH ENERGY-DISPERSIVE X-RAY SPECTROSCOPY (SEM-EDS)

A comprehensive morphological and microchemical investigation of all the samples analysed (H1–H8) was performed using SEM-EDS. The examination of non-conductive three-dimensional samples was carried out under variable pressure mode (30 Pa) at an accelerating voltage of 20 kV, with applied magnifications ranging from 1.0 × 10^2 to 3.2 × 10^4. The analyti-

cal procedures were conducted using a *Zeiss Sigma VP* field emission scanning electron microscope, ensuring high-resolution imaging combined with precise elemental characterisation. The SEM-EDS analyses described were performed at the Environmental Cryo-SEM Low Temperature Scanning Electron Microscopy Laboratory of the Department of Geology, Warsaw University.

RAMAN SPECTROSCOPY (RS)

RS was performed on seven samples (H2–H8). The Raman mechanism is characterised by the inelastic scattering of laser light by molecules in the sample under investigation. This process culminates in the emission of a photon with a modified frequency, thereby reflecting variations in the energy levels of molecular vibrations. The shift in wave numbers (cm^{-1}) facilitates the identification of specific bonds and functional groups. The clay samples were prepared as a thin layer and applied to a microscope slide. A Renishaw in ViaQontorInSpect Raman microscope, equipped with a 785-nm wavelength laser, was used for the analyses, which facilitated the reduction of ferrous phase fluorescence. The laser power was set in the range 1–5 mW and the acquisition time was 5–10 s, with 3–5 acquisitions per point.

The mapping of mineral phases was facilitated by a confocal microscope with a spatial resolution of approximately 1 µm. The RS and SEM-EDS analyses were performed at the Environmental Cryo-SEM Low Temperature Scanning Electron Microscopy Laboratory, which is managed by the Faculty of Geology at the University of Warsaw.

RESULTS

GRAIN-SIZE CHARACTERISTICS

The preponderance of silt and clay fractions in all samples suggests a low-energy sedimentation environment (Table 1 and Fig. 3). The minimal sand content observed indicates the absence of a significant supply of coarse material, showing that deposition occurred under conditions of limited water flow (Zieliński, 2014).

Sample H7 is characterised by a higher proportion of particles with a diameter smaller than 2 µm (64.3 vol.%) and the smallest average grain size (4.9 µm). This is also true for samples H2–H6 and H8. They contained 76–89 vol.% silt fraction, 11.9–22.9 vol.% clay fraction and only 0–2 vol.% of sand grains (Table 1). Sample H1 was an exception, in which organic matter was found, as confirmed by H_2O_2 treatment.

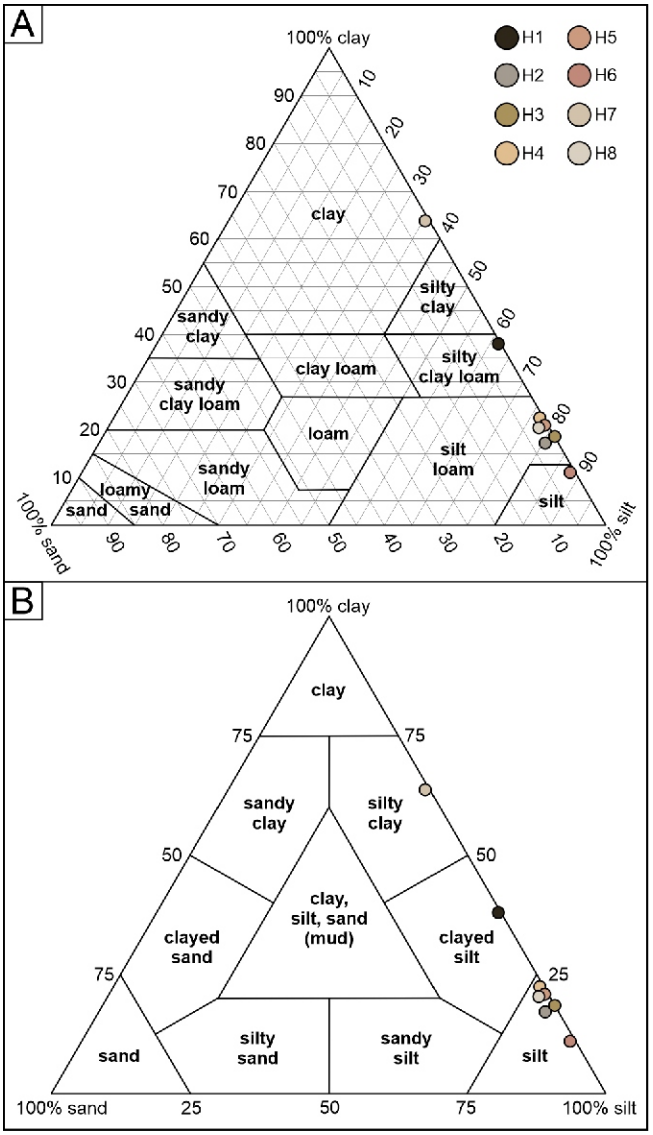

Fig. 3. Grain-size distribution and nomenclature of samples H1–H8 using different classifications

A – *according to the USDA classification system (Retallack, 2019); **B** – **according to the classification scheme of Shepard (1954); for details of grain-size distribution, see Table 1

Table 1

Results of grain-size analysis of the samples examined

Sample	Sediment grain size [vol.%]			Mean grain size [µm]	Soil name*	Sediment name**
	clay <2 µm	silt 2–63 µm	sand >63 µm			
H1	37.15	62.48	0.37	6.60	silty clay loam	clayed silt
H2	16.98	80.97	2.05	8.50	silt loam	silt
H3	17.87	82.13	0.00	8.20	silt loam	silt
H4	22.89	76.47	0.64	7.60	silt loam	silt
H5	21.00	78.3	0.70	8.30	silt loam	silt
H6	11.87	89.2	0.98	9.90	silt	silt
H7	64.32	35.89	0.01	4.90	clay	silty clay
H8	20.85	78.29	0.86	8.50	silt loam	silt

For sediment name in different classifications, see Figure 3

Table 2

Mineralogy of the samples examined based on quantitative analysis using the Rietveld method

Sample / Mineral	H1	H2	H3	H4	H5	H6	H7	H8
quartz	42.00% (53)	66.00% (82)	31.34% (31)	58.7% (76)	61.81% (79)	47.07% (62)	15.58% (19)	40.38% (48)
"illite"	18.07% (72)	14.09% (54)	21.96% (75)	16.4% (60)	14.43% (27)	16.48% (68)	8.07% (21)	14.5% (48)
smectite-group representative	15.17% (68)	6.64% (46)	9.57% (54)	4.84% (35)	5.09% (46)	6.35% (55)	8.48% (45)	7.89% (43)
chlorite-group representative	–	–	–	2.37% (27)	0.7% (14)	–	–	–
orthoclase	5.46% (46)	1.84% (43)	3.48% (47)	3.00% (53)	1.85% (39)	4.37% (49)	1.79% (51)	6.04% (36)
microcline	–	–	4.96% (47)	2.84% (38)	–	–	5.15% (68)	–
albite	–	–	0.63% (58)	–	–	–	2.33% (73)	–
kaolinite	11.22% (13)	8.11% (60)	28.06% (97)	8.21% (46)	13.73% (56)	23.7% (47)	8.47 % (31)	21.81% (58)
gypsum	2.87% (24)	–	–	–	–	–	0.78% (17)	5.07% (36)
calcite	–	–	–	–	–	–	49.35% (75)	–
anatase	0.39% (21)	0.72% (17)	–	–	–	–	–	1.52% (45)
goethite	4.82% (75)	–	–	3.17% (87)	0.8% (54)	–	–	0.53% (53)
hematite	–	–	–	–	1.59% (75)	1.5% (64)	–	–
jarosite	–	2.60% (43)	–	–	–	–	–	2.26% (34)
pyrite	–	–	–	0.47% (24)	–	0.53% (54)	–	–
Total counts	100% (372)	100% (392)	100% (485)	100% (446)	100% (390)	100% (399)	100% (400)	100% (468)

MINERAL COMPOSITION

The quantitative PXRD analysis was conducted using the Rietveld method (Rietveld, 1969). This technique enabled the identification and determination of the crystal phase proportions in samples H1–H8. The following minerals were identified, based on the fitting of diffraction spectra: quartz, “illite”, minerals from the smectite and chlorite groups, orthoclase, microcline, albite, kaolinite, gypsum, calcite, anatase, goethite, hematite, jarosite and pyrite (Table 2). The presence of these minerals was confirmed on the basis of characteristic diffraction positions and intensity profile matching. The term “illite” is employed here as a conventional designation for dioctahedral, non-expanding, clay-sized micaceous minerals. Despite its non-approval by the International Mineralogical Association (IMA) and its frequent association with fine-grained muscovite, the term is maintained in this study due to its well-established use in geological literature.

The most prevalent phase was quartz, whose content ranged from 15.58% (in sample H7) to 66.00% (in sample H2). High proportions of this mineral were observed, especially in samples H2, H4 and H5, indicating the dominance of a strongly siliceous component in the parent material. The second most prevalent phase was “illite”, which was detected in all samples in the range 8.07–21.96%. “Illite” is a characteristic component of the clay fraction (Środoń et al., 2014). Additionally, smectite was identified in all of the samples, with a maximum content of 15.17% in sample H1 (Table 2).

Of particular interest is kaolinite. Its highest proportion was found in sample H3 (28.06%). Elevated contents were also noted in samples H6 (23.70%) and H8 (21.81%). Furthermore, a substantial proportion of calcite (49.35%) was identified in sample H7 (Table 2).

Aluminosilicates, including orthoclase and microcline, were sporadically distributed. For example, microcline showed its highest content in sample H7 (5.15%), while albite was only present in samples H3 and H8 in trace amounts, i.e. below 2.5%. Secondary phases, including gypsum, anatase, goethite, hematite, jarosite and pyrite, were present in limited amounts and with spatial variation. Goethite was predominantly present in samples H1, H4 and H5, while jarosite was detected in samples H2 and H8 (Table 2).

Table 3

Statistical parameters of individual samples: Rietveld method

Sample	R_{wp} [%]	R_{exp} [%]	GoF
H1	11.93	2.55	4.6784
H2	9.87	2.87	3.439
H3	4.97	2.35	2.1149
H4	7.01	2.41	2.9087
H5	6.50	2.27	2.8634
H6	5.95	2.37	2.5105
H7	8.56	3.56	2.4045
H8	7.89	2.73	2.8901

R_{wp} – weighted profile R-factor, R_{exp} – expected R-factor, GoF – Goodness of Fit

The quality of the model fit to the experimental data was assessed based on the R_{wp}, R_{exp}, and GoF parameters (Table 3). R_{wp} values ranged from 4.97% in sample H3 to 11.93% in sample H1, while GoF values ranged from 2.11 to 4.68. The optimal fit was identified for sample H3 (GoF = 2.11). By contrast, the most significant mismatch was observed for sample H1 (GoF = 4.68; Table 3). This may be potentially attributable to the presence of amorphous phases or the incomplete alignment of background parameters.

IRON PHASES

^{57}Fe-MS analysis of samples H1–H8 indicated a diverse speciation of iron, including: Fe^{3+}-containing oxide/oxyhydroxide nanophases, Fe^{3+} in silicates (primarily “lillite”, muscovite, kaolinite and chlorite) and trace amounts of Fe^{2+} in silicates (Fig. 4 and Table 4). In samples H5 and H6, distinct hematite components were identified, characterised by the presence of hyperfine fields of 48–50 T, thereby confirming the

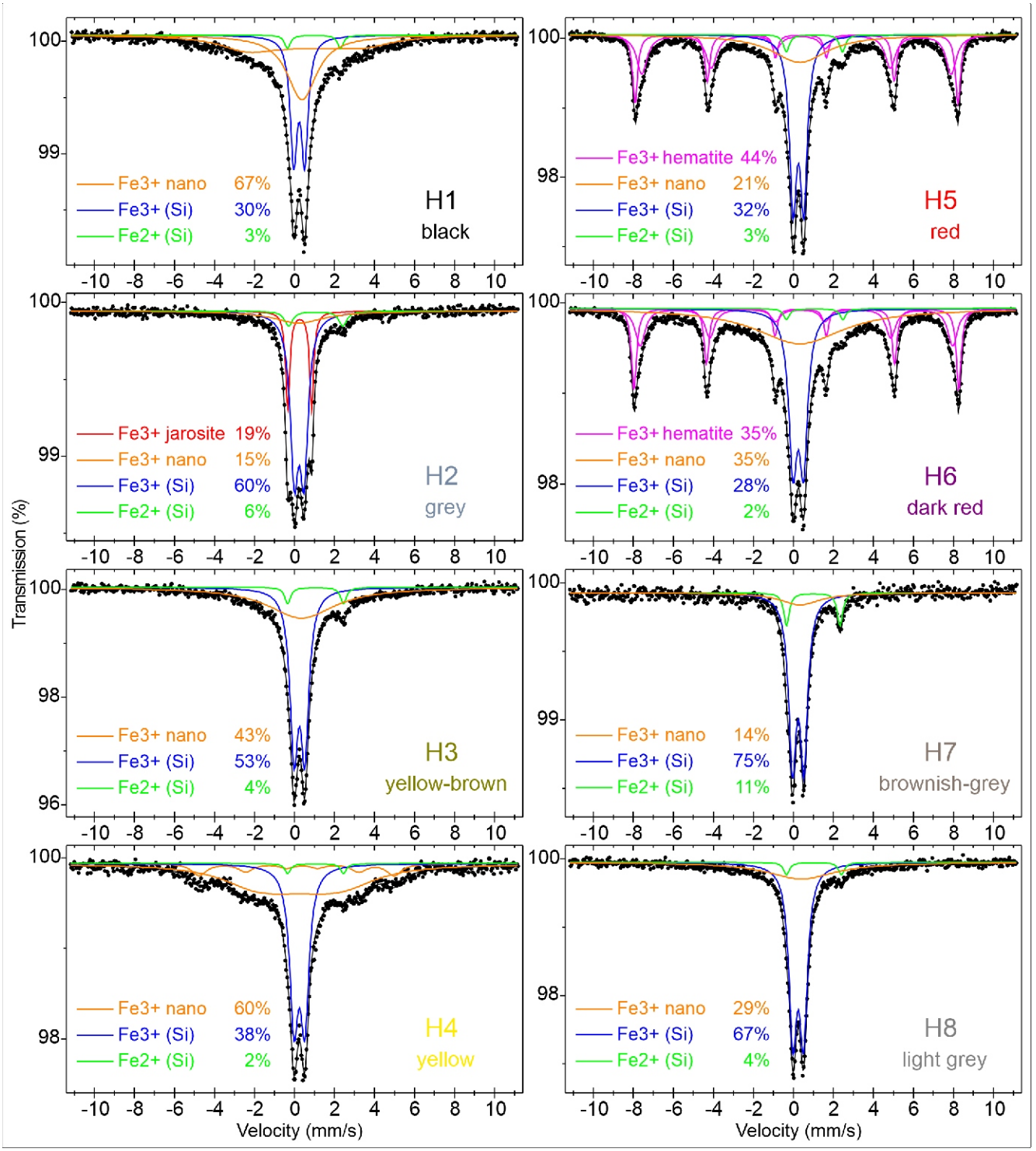

Fig. 4. ^{57}Fe Mössbauer spectra of the samples analysed from the Honoratka dump

presence of a well-crystallised (bulk) magnetically ordered phase. In most cases, Fe-containing minerals were identified as nanocrystals in this study. The ^{57}Fe Mössbauer spectra showed a substantial broadening of the spectral line width. This phenomenon can be attributed to the superparamagnetic relaxation of electron spins within the magnetic domains of the nanoparticles. The relaxation rate is contingent upon two factors: crystallinity (which is defined as the particle size) and temperature. It is widely accepted that the upper size limit for nanocrystals, below which superparamagnetism occurs at room temperature, is ~10 nm (Schwertmann, 1993; Murad and Cashion, 2004; Murad, 2010).

The isomer shift values for Fe^{3+} in silicates ranged from 0.35 to 0.37 mm/s, while the quadrupole splitting reached 0.48–0.57 mm/s. These findings indicate the dominance of Fe^{3+} ions in an octahedral environment with moderately distorted symmetry. The Fe^{2+} minerals, present in trace amounts (2–11%), show higher Fe^{2+}-specific IS values (approximately 1.1–1.2 mm/s) and Fe^{2+}-specific QS values (2.6–2.8 mm/s), which are characteristic of layered silicates (Fig. 4 and Table 4).

The content of oxide/oxyhydroxide nanophases varies, ranging from 14% (H7) to 50% (H4), suggesting significant disparities in the degree of fragmentation and crystallinity of the materials under study. Of particular interest is the presence of

Table 4

^{57}Fe Mössbauer spectroscopy parameters of samples from the Honoratka dump

Sample	Fe-bearing phase	A (%)	IS (mm/s)	QS (mm/s)	*B* (Tesla)	Γ_a (mm/s)
H1	Fe^{3+} silicates	30	0.35	0.55	–	0.41
	Fe^{2+} silicates	3	1.09	2.64	–	0.35
	Nano-hematite	35	0.5	–	–	2
		32	0.3	–	19	3
H2	Fe^{3+} jarosite	19	0.37	1.19	–	0.25
	Fe^{3+} silicates	60	0.35	0.48	–	0.49
	Fe^{2+} silicates	6	1.17	2.71	–	0.5
	Nano-hematite	15	0.3	–	–	3
H3	Fe^{3+} silicates	53	0.36	0.54	–	0.48
	Fe^{2+} silicates	4	1.17	2.79	–	0.35
	Nano-goethite	43	0.47	–	–	4
H4	Fe^{3+} silicates	38	0.36	0.53	–	0.51
	Fe^{2+} silicates	2	1.17	2.79	–	0.35
	Nano-goethite	50	0.4	–	15	4
		10	0.36	–0.3	30.2	0.9
H5	Fe^{3+} hematite	19	0.38	–0.21	50.06	0.3
		25	0.37	–0.21	48	0.63
	Fe^{3+} silicates	32	0.36	0.53	–	0.43
	Fe^{2+} silicates	3	1.17	2.8	–	0.35
	Nano-hematite	21	0.4	–	–	3
H6	Fe^{3+} hematite	18	0.37	–0.21	50.33	0.3
		17	0.36	–0.2	48.4	0.58
	Fe^{3+} silicates	28	0.35	0.53	–	0.5
	Fe^{2+} silicates	2	1.17	2.83	–	0.35
	Nano-hematite	35	0.4	–	–	5
H7	Fe^{3+} silicates	75	0.35	0.57	–	0.45
	Fe^{2+} silicates	11	1.11	2.67	–	0.32
	Nano-goethite	14	0.5		–	2
H8	Fe^{3+} silicates	67	0.35	0.52	–	0.47
	Fe^{2+} silicates	4	1.14	2.74	–	0.35
	Nano-hematite	29	0.5	–	–	4

A – relative area of spectral component (the distribution of iron atoms in Fe-bearing minerals), IS – isomer (center) shift relative to -Fe, QS – quadrupole splitting, – hyperfine magnetic field, and – spectral line-width (FWHM – full width at half maximum). Errors are of the order of unity for the last digit shown

jarosite in sample H2. In addition, a hematite component was identified in two samples (H5 and H6). These samples exhibit an isomer shift of 0.37 mm/s, quadrupole splitting of –0.2 mm/s and a hyperfine field of ~50 T, which is typical for this phase (Fig. 4 and Table 4). The content of oxide/oxyhydroxide ranges from about ten to several tens percent.

SELECTED COLOURING MINERALS

The SEM-EDS analysis was employed to help with comprehensive identification of the mineral composition and potential phases responsible for the colouration of the samples H1–H8 (see Fig. 2). The results indicate significant mineralogical variability, primarily involving iron minerals (oxides, hydroxides, and sulphates) and titanium oxides (Figs. 5 and 6).

In sample H1, which is black, the presence of anatase (TiO_2) and goethite (FeO(OH)) occurred in the form of finely crystalline clusters with irregular contours. The grey sample, H2, showed the coexistence of anatase (tetrahedral structure) and jarosite ($KFe_3(SO_4)_2(OH)_6$). The jarosite aggregates observed in the SEM image manifest as small, irregular clusters, locally coexisting with titanium phases (Mameli et al., 2007). In the case of the sample H3, which was yellow-brown, the minerals responsible for its colour could not be clearly identified. The EDS analyses showed the presence of iron, sulphur, and oxygen but without clear signatures indicating specific mineral phases. The observed colouration may be attributable to a mixture of finely dispersed amorphous phases or weakly crystalline products of iron weathering (Cuadros et al., 2020).

Sample H4 had a distinct yellow hue (see Fig. 2) and was found to contain pyrite (FeS_2) and goethite. Pyrite manifests in the form of isometric crystals (Fig. 5). Sample H5, of red hue, predominantly comprised goethite and hematite (Fe_2O_3). Fine, compact aggregates of these minerals have been observed, commonly forming transitional textures between hydrated and dehydrated forms of iron (Fig. 6). In the case of sample H6, characterised by its dark red colouration, coexistence of hematite and pyrite was observed.

For sample H7, brownish-grey similar to sample H3, the minerals responsible for the observed colouration could not be unambiguously identified. The chemical composition of the surface indicated the presence of iron and oxygen. However, the lack of clear peaks in the EDS spectra precluded assigning them to specific phases. As indicated by the presence of anatase, goethite, and jarosite, sample H8, of light grey colouration, was composed of these mineral phases (Fig. 6).

MINERAL AND ORGANIC PHASES

RS analysis of samples H2–H8 enabled the unambiguous identification of the predominant mineral phases present in the Poznań Clays (Table 5). Sample H1 was not analysed due to its

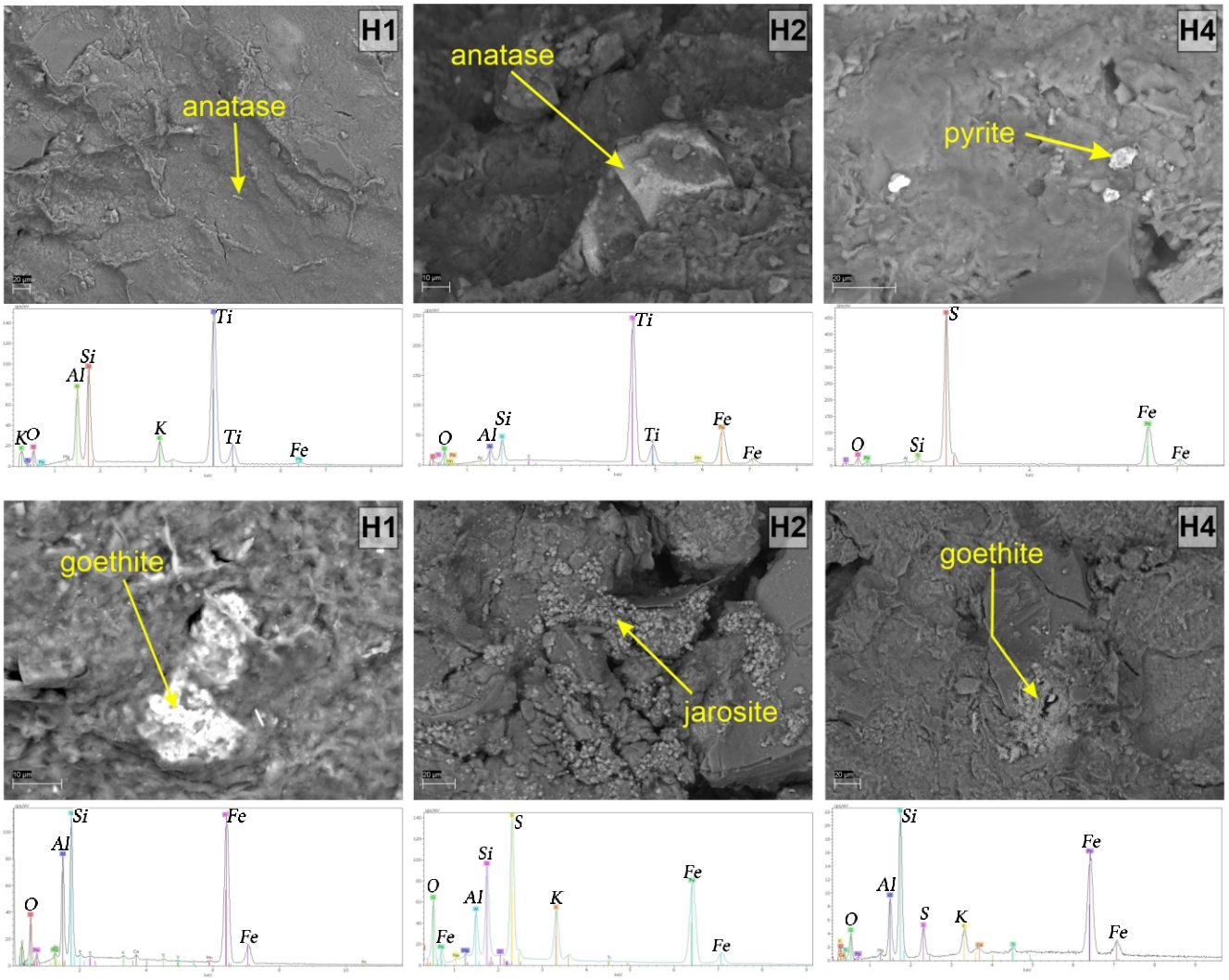

Fig. 5. Representative SEM images of samples H1, H2 and H4, with EDS spectra showing local elemental compositions

high organic matter content, which prevented the acquisition of reliable Raman spectra. The spectra recorded showed bands indicative of quartz, hematite, goethite and calcite, along with signals associated with the presence of organic matter. In several cases, weak indications of clay minerals, such as "illite" and kaolinite, were also noticeable.

The most diagnostic quartz band (~464 cm^{-1}) occurred in many samples, including H2_1, H3_2, H3_5, H3_7, H4_1, H4_2, H4_5, H5_2, H5_5, and H6_5. Its identification was confirmed by additional bands in the range 127–209 cm^{-1} and 396–401 cm^{-1}. Quartz is a prevalent detrital sedimentary component and intense bands were recorded in the range 1575–1581 cm^{-1} in samples H2_2, H3_4, H3_6, and H3_8. These bands correspond to the so-called G-band of graphite and carbonaceous substances. The presence of these signals is indicative of preserved organic matter, most likely associated with lignite and kerogen present in the Poznań Clays studied (Table 5).

Characteristic bands of hematite (219–278 cm^{-1}, 625 cm^{-1} and overtones in the range 1305–1320 cm^{-1}) were recorded in many samples, including H3_1, H3_2, H3_3, H3_5, H3_9, H4_3, H5_1, H6_1–H6_4, H7_1, H8_1, and H8_2. Bands within the 650–700 cm^{-1} range (indicative of goethite) were identified in samples H4_4, H6_1, and H6_2. In several samples, such as H5_2 (band 143 cm^{-1}), signals were recorded that may depict the presence of kaolinite or "illite" (Table 5). However, due to the overlap of bands with dominant phases, this identification remains uncertain.

DISCUSSION

GRAIN SIZE, ENVIRONMENT AND COLOUR CONTROLS

The grain size distribution of samples H1–H8 from the Honoratka dump indicates a predominance of silt and clay (cf. Fig. 3 and Table 1), indicating a low-energy environment (Widera, 2013; Widera et al., 2017, 2019; Zieliński, 2014). Nevertheless, their mixture, locally with an admixture of sand, suggests sudden deposition (Zieliński and Widera, 2020; Urbański et al., 2025). Alternatively, the sand grains may be aeolian (e.g., Środoń et al., 2001, 2014), though this possibility has not yet been either confirmed or excluded.

The relatively high clay content in samples H1 and H7 may suggest local clay sources or secondary pedogenic and diagenetic processes promoting accumulation of the <2 μm fraction. These processes typically increase illitisation and alter the degree of "illite" ordering. "Illite" crystallinity was not quanti-

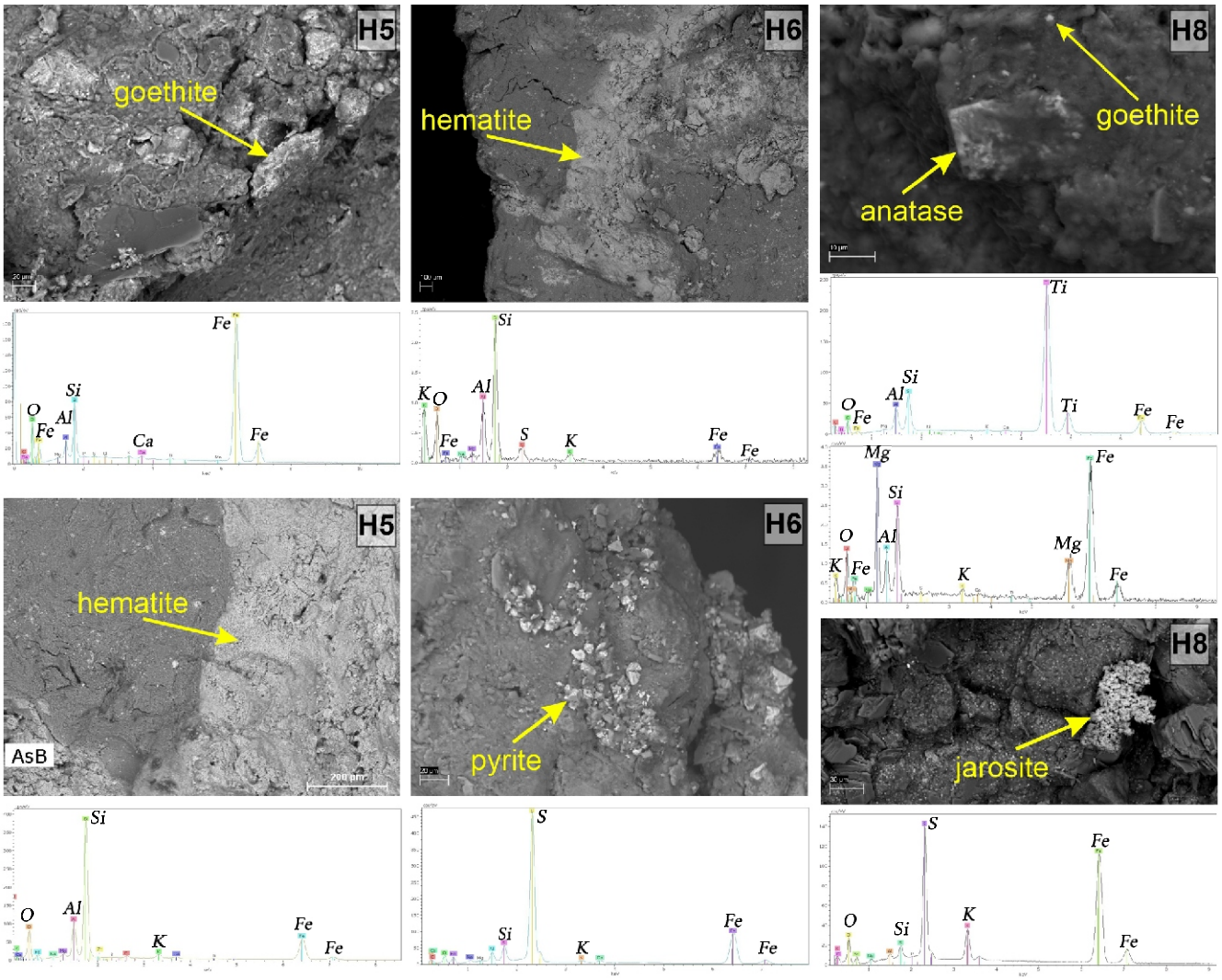

Fig. 6. Representative SEM images of samples H5, H6 and H8, with EDS spectra showing local elemental compositions

fied in this study; however, the fine grain size of the sediment clearly limited pore-water circulation. This limited circulation exerted a strong control over Eh levels (~ –0.2 to +0.2 V at pH 6–7) and pH levels (nearly neutral to slightly acidic), which were constrained, thereby limiting iron mineral stability fields and, consequently, the colour patterns observed. This finding aligns with experimentally and thermodynamically derived Eh–pH relations for iron minerals (Walker, 2018).

RELATIONSHIPS BETWEEN COLOUR, MINERAL PHASES AND REDOX CONDITIONS

The colour variation of samples H1–H8 is attributable to the interaction of mineral phases, redox conditions and the presence of organic matter (Duczmal-Czernikiewicz, 2010; Maciaszek et al., 2019, 2020; TCMS, 2022; Klęsk et al., 2023). However, all specimens investigated were collected from an anthropogenic dump, a setting where recent weathering, oxidation and partial reworking are known to modify the original mineral assemblages and colour patterns of clayey deposits. Consequently, the inferred Eh–pH conditions discussed below should be regarded as qualitative indicators of prevailing palaeoenvironmental trends rather than as precise reconstructions of the primary diagenetic regime.

The black shades observed in sample H1 are indicative of low Eh and the presence of amorphous phases of organic matter. The high muscovite and goethite contents may have modulated the tone of the sediment but organic matter played a dominant role (Bown and Kraus, 1981, 1987).

The grey tones which are characteristic of samples H2, H7, and H8 are attributable to the prevalence of quartz and “illite” in the absence of significantly pigmented phases (cf. Fig. 2 and Table 2). The elevated pH level promoted the stability of Fe^{3+} silicates, whilst mitigating the intensity of the resulting colours. In the case of sample H8, the white and pale shades are indicative of high calcite and kaolinite contents, suggesting their formation under conditions of neutral to moderately oxidising conditions (Valanciene et al., 2010; Mancini et al., 2020). On the other hand, the presence of the khaki colour in sample H3 is attributed to the overlap of Fe^{3+} and Fe^{2+} pigmentation in silicates, suggesting slightly acidic and oxidising local conditions (Albee and Chodos, 1970).

Table 5

Compilation of band positions and chemical (mineral) assignments obtained after background correction and normalisation of Raman spectra for the samples from the Honoratka dump

Sample	Positions (cm^{-1})	Phase interpretation
H2_1	127, 207, 464	quartz
H2_2	1579	organic matter
H3_1	153, 219, 276, 625, 1320	hematite
H3_2	218, 276, 396, 463, 1313	quartz + hematite
H3_3	216, 274, 401, 1310	hematite
H3_4	1581	organic matter
H3_5	216, 278, 399, 466, 620, 1305	quartz + hematite
H3_6	1575	organic matter
H3_7	218, 274, 459	quartz + possible hematite
H3_8	1575	organic matter
H3_9	215, 277, 398	hematite
H4_1	128, 209, 464	quartz
H4_2	464	quartz
H4_3	217, 278, 398, 1320	hematite
H4_4	150, 287, 409, 561, 704, 797	goethite
H4_5	464	quartz
H5_1	217, 278	hematite
H5_2	143, 463	quartz + possible kaolinite
H6_1	224, 294, 406, 604, 661, 702, 1317	hematite + goethite
H6_2	217, 261, 394, 652, 698, 1011, 1306	hematite + goethite
H6_3	214, 274, 398, 1313	hematite
H6_4	215, 274, 401, 1314	hematite
H6_5	127, 207, 394, 464	quartz
H7_1	212, 274, 391	hematite
H8_1	215, 285, 398, 1318	hematite
H8_2	217, 272	hematite

The yellow tones that are characteristic of sample H4 are associated with the presence of goethite crystallising in an oxidising environment at neutral or slightly acidic pH. Similar relationships between hematite-rich assemblages, red colouration and oxidising marine or terrestrial environments have been documented in studies of red beds (e.g., Torrent et al., 1980; Bown and Kraus, 1981).

The red tones present in the samples H5 and H6 are attributable to the presence of hematite (cf. Figs. 2 and 6, and Tables 2, 4, and 5), which is known to form under conditions of elevated Eh and neutral pH (Bown and Kraus, 1987; Tucker, 2003). In sample H6, the presence of a darker purple tone suggests a higher proportion of well-crystallised hematite or the potential presence of anatase and Fe^{2+} (Tucker, 2003). Yellow and yellow-brown tones, linked to goethite and early jarosite in this study, are consistent with observations from incipiently reddened carbonate and siliciclastic successions, where low-temperature oxidative alteration produces patchy yellow-pink hues (Turner, 1980; Tucker, 2011; Upreti and Srivastava, 2019). Nevertheless, for all colour types, the possible superposition of late-stage oxidative alteration on the dump implies that our colour–Eh–pH interpretations should be viewed as minimum estimates of the original redox gradients operating in the Poznań Clays.

REDOX CONDITIONS AND COLOUR EVOLUTION

The colour of the Poznań Clays is directly influenced by the redox conditions (Eh) and the pH of the environment. Lower Eh values have been shown to promote the preservation of organic matter, the formation of dark shades and the crystallisation of pyrite. Conversely, high Eh stimulates the crystallisation of hematite and goethite, giving red and yellow hues to the deposits. It has been demonstrated that the lowering of pH promotes the formation of jarosite, which is responsible for the observed yellowish tones (Wiewióra and Wyrwicki, 1974, 1976). By contrast, neutral to alkaline conditions have been shown to ensure the stability of calcite and kaolinite, which serve to lighten the colours of the deposits. The inferred sequence from pyrite, under reducing conditions, to jarosite and other Fe sulphates, under acidic oxidising conditions, mirrors the experimental and field constraints on iron sulphide stability and oxidation (Nordstrom, 1982).

Secondary transformations of iron-bearing phases, especially the oxidation of pyrite and the transition of goethite to hematite, greatly influence sediment colour during diagenesis. Under reducing conditions (low Eh, the absence of dissolved oxygen, and pH 6–8), pyrite (FeS_2) is stable. However, upon exposure to oxidising pore waters (positive Eh, pH 5–8), pyrite is converted into sulphate and Fe^{3+} phases. This process can be expressed schematically, as follows:

$$FeS_2 \quad \frac{15}{4}O_2 \quad \frac{7}{2}H_2O \quad Fe(OH)_3(s) \quad 2SO_4^2 \quad 4H$$

The resulting Fe^{3+} hydrolyses and progressively transforms into more crystalline Fe^{3+} oxyhydroxides and oxides:

$$Fe^3 \quad 3H_2O \quad Fe(OH)_3(s) \quad 3H$$

$$Fe(OH)_3(s) \quad FeO(OH)(goethite) + H_2O$$

$$2FeO(OH)(goethite) \quad Fe_2O_3\ (hematite) + H_2O$$

The appearance of a symbol (s) in close proximity to a given chemical formula is an indication that the substance in question exists as a solid phase (i.e. a precipitate or mineral).

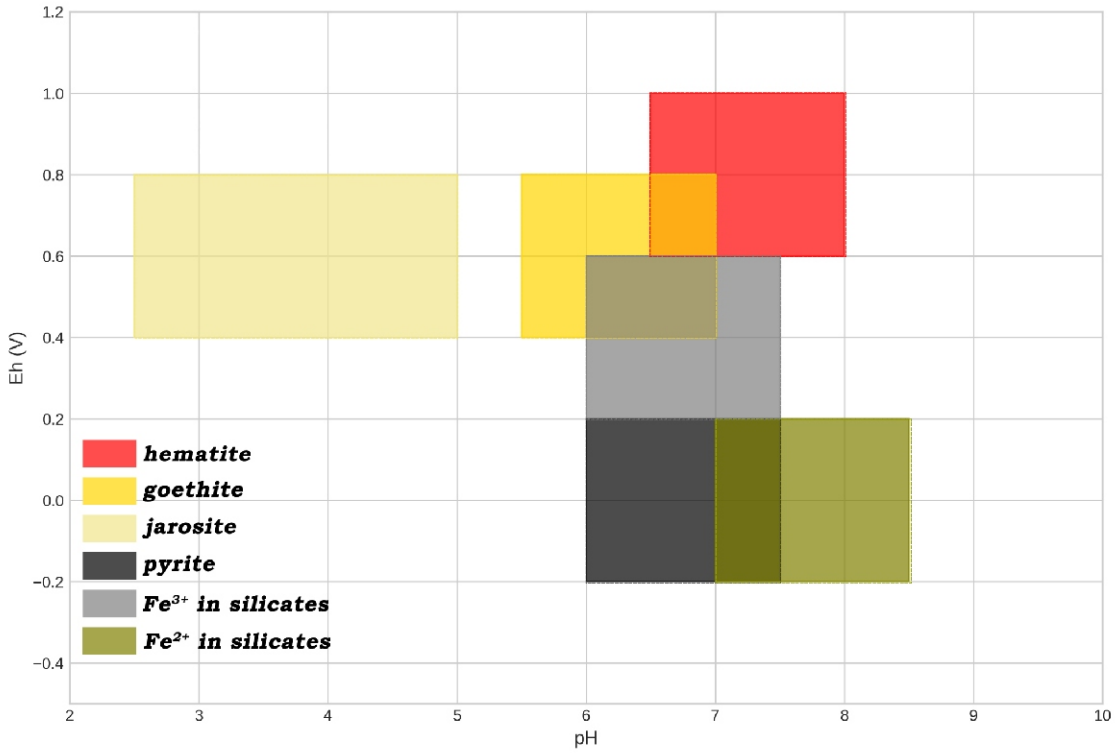

Fig. 7. Eh–pH diagram showing the stability fields of iron phases according to Brookins (2012)

Goethite represents an intermediate mineral, between amorphous or poorly crystalline Fe^{3+} hydroxides and well-ordered hematite. Both minerals are stable over a broad pH range (4–8) under oxidising conditions. However, goethite forms preferentially in cooler, more humid settings, while hematite forms in warmer, periodically dry environments that enhance goethite's dehydroxylation. This sequence defines a geochemical "colour pathway": from grey to black or greenish hues, in reducing conditions dominated by sulphides and Fe^{2+} bearing carbonates and silicates, to yellow and yellow-brown tones, where ferrihydrite and goethite prevail at pH 4–8 and positive Eh, to intense red colours in well-oxidised, warmer and drier settings, where hematite becomes the dominant pigment.

However, even minimal amounts of pigmenting phases can dominate over neutral mineral components (e.g., quartz, clay minerals, etc.; Nemec and Porębski, 1977; Klęsk et al., 2023), as shown by observations from SEM-EDS and ^{57}Fe-MS analyses (Kraus and Riggins, 2007; Kruszewski, 2013). ^{57}Fe-MS data clearly shows the correlation between the proportion of hematite and the intensity of red and purple colours, as well as between the presence of goethite and yellow shades. Moreover, as indicated by the SEM-EDS results, the spatial distribution of colour-forming phases is highlighted by even minimal amounts of hematite or jarosite (cf. Figs. 5 and 6).

RS was used to confirm the presence of hematite and goethite as primary pigments. Additionally, the analysis revealed signals of organic matter that indicate the presence of dark shades (see Table 5). Thus, the use of several analytical methods allows for a more complete understanding of the colour-forming processes and their dependence on environmental variables, such as Eh and pH (Fig. 7).

PIGMENTING PHASE DISTRIBUTION

Sedimentary colour is the result of the complex interplay between the mineral phases present, their content, degree of crystallinity and distribution in the samples examined. It has been clearly demonstrated that even minimal amounts of strongly pigmented phases, mainly hematite and goethite, can exert a dominant influence on sedimentary colour. A good example of this phenomenon seems to be the presence of fine-grained goethite, which, despite its minimal content, gives the sediment a distinct yellow hue (Huang and Zhang, 2020). However, structural studies of the Poznań Clays characterised the role of nanocrystalline iron oxyhydroxides, layered double hydroxides (including green rust-type phases) and Fe-rich smectites as transition pigments and redox buffers (e.g., Wyrwicki, 1969, 1974, 1975; Wyrwicki and Wiewióra, 1981).

CONDITIONS OF IRON PHASE STABILITY

The Eh–pH relationship enables graphical presentation of the stability of iron phases and their corresponding colours (Fig. 7). The lower middle part of the diagram, corresponding to Eh values of ~ –0.2 to 0.2 V and near-neutral pH of about 6–7, represents the stability field of pyrite and the presence of organic matter, giving gray to black tones. The upper left-hand corner of the diagram, corresponding to elevated Eh values of ~0.4–0.8 V and acidic pH of roughly 2.5–5.0, is associated with jarosite, a mineral responsible for the yellow colouration observed. The central area, characterised by a medium Eh and neutral pH, corresponds to goethite, which is responsible for the yellow and brown shades. The upper middle part of the diagram, which corresponds to a high Eh and neutral pH, is associated with hematite, a mineral that yields red and purple hues. On the other hand, the lower middle part of the diagram covers calcite and kaolinite, which are known to produce light to pale shades in sediment (Fig. 7).

The diagram characterised above bears a resemblance to the classic Pourbaix diagrams, in which the boundaries of iron phase stability are not only determined by the presence of pigments but, also, by their secondary transformations. The proposed Eh–pH-colour framework for the Poznań Clays is consistent with Pourbaix-type stability relationships for Fe minerals

and with broader models of the evolution of marine and continental red beds (e.g., Torrent et al., 1980; Bown and Kraus, 1981, 1987; Zachos et al., 2001; Zatoń et al., 2008; Bábek et al., 2021). Thus, in the case of the Poznań Clays, the colour scheme is a direct reflection of the geochemical conditions, primarily Eh and pH, which controlled the forms of iron and their subsequent transformations.

CONCLUSIONS

1. The main factor influencing the colouration of the Poznań Clays is the presence of ferric phases such as hematite, goethite or jarosite. Hematite is responsible for the intense red and purple colours observed in samples H5 and H6. Goethite is the source of the yellow and brown hues that are characteristic of samples H3 and H4. Jarosite gives the yellowish and greyish yellow colours of samples H2 and H8.
2. These pigmenting minerals are sensitive indicators of redox and pH conditions during deposition of the Poznań Clays and their diagenetic processes. Hematite indicates oxidising conditions with high Eh and pH near to neutral, goethite is characterised by medium Eh and neutral pH, while jarosite is indicative of acidic and strongly oxidising conditions: medium Eh and low pH.
3. Sample H7, and also samples H2 and H8 to a certain extent, do not contain (or are depleted) in these pigments and relatively enriched in quartz and "illite" or calcite and kaolinite; hence their grey tones. Sample H1 is black because of the organic matter dispersed in it, although it contains the largest amounts of strongly pigmenting goethite.
4. Finally, the results obtained in this study clearly show changing palaeoenvironmental conditions recorded in the colour of the Poznań Clays. The reconstructed Eh and pH values indicate water level fluctuations on floodplains, resulting most likely from climatic changes during the late Neogene in the Polish Lowlands area.

Acknowledgements The authors would like to thank Dr. Iwona Dobak-Sroka of the Environmental Laboratory for Unique Chemical Instrumentation at the Faculty of Chemistry, Adam Mickiewicz University in Poznań, for her PXRD analyses. Finally, we would like to express our profound gratitude to the reviewers for their invaluable contributions to enhancing our manuscript.

REFERENCES

Albee, A.L., Chodos, A.A., 1970. Semiquantitative electron microprobe determination of Fe^{2+}/Fe^{3+} and Mn^{2+}/Mn^{3+} in oxides and silicates and its application to petrologic problems. American Mineralogist, **55**: 491–501.

Areń, B., 1964. Geological atlas of Poland: stratigraphic and facies problems. Tertiary, 11/a. Wydaw. Geol., Warszawa.

Bábek, O., Vodrážková, S., Kumpan, T., Kalvoda, J., Holá, M., Ackerman, L., 2021. Geochemical record of the subsurface redox gradient in marine red beds: a case study from the Devonian Prague Basin, Czechia. Sedimentology, **68**: 3523–3548; https://doi.org/ 10.1111/sed.12910

Badura, J., Przybylski, B., 2004. Evolution of the Late Neogene and Eopleistocene fluvial system in the foreland of the Sudetes Mountains, SW Poland. Annales Societatis Geologorum Poloniae, **74**: 43–61.

Bąk, K., Bąk, M., Gatlik, J., Błachowski, A., 2020. Oscillating redox conditions in the Middle–Late Jurassic Alpine Tethys: insights from selected geochemical indices and ^{57}Fe Mössbauer spectroscopy. Palaeogeography, Palaeoclimatology, Palaeoecology, **537**, 109440; https://doi.org/10.1016/j.palaeo.2019.109440

Błachowski, A., Ruebenbauer, K., Żukrowski, J., Górnicki, R., 2008. Early design stage of the MsAa-4 Mössbauer spectrometer. Acta Physica Polonica A, **114**: 1707–1713; https://doi.org/10.12693/APhysPolA.114.1707

Blott, S.J., Pye, K., 2001. Gradistat: a grain size distribution and statistics package for the analysis of unconsolidated sediments. Earth Surface Processes and Landforms, **26**: 1237–1248; https://doi.org/10.1002/esp.261

Bojakowska, I., Barański, P., Iwasińska-Budzyk, I., Retka, J., 2010. Variability of the content of trace elements in Poznań series clays (in Polish with English summary). Górnictwo i Geologia, **5**: 31–39.

Bown, T.M., Kraus, M.J., 1981. Lower Eocene alluvial paleosols (Willwood Formation, Northwest Wyoming, U.S.A.) and their significance for paleoecology, paleoclimatology, and basin analysis. Palaeogeography, Palaeoclimatology, Palaeoecology, **34**: 1–30; https://doi.org/10.1016/0031-0182(81)90056-0

Bown, T.M., Kraus, M.J., 1987. Integration of channel and floodplain suites, I. Developmental sequence and lateral relations of alluvial paleosols. Journal of Sedimentary Petrology, **57**: 587–601; https://doi.org/10.1306/212F8BB1-2B24-11D7-8648000102C1865D

Brookins, D.G., 2012. Eh-pH diagrams for geochemistry. Springer Science & Business Media.

Card, C.J., Montenari, M., 2023. Comparative geochemistry of Early Carboniferous marine red beds (MRBs) and their significance for deep time paleoceanographic reconstructions. Sedimentary Geology, **444**, 106313; https://doi.org/10.1016/j.sedgeo.2022.106313

Choma-Moryl, K., 1988. Variability of physical properties of the Poznań Clays from the area of Wrocław, with reference to their genesis and lithostratigraphy. Geologia Sudetica, **23**: 1–63.

Christiansen, B.C., 2004. A transformational, structural and natural occurrence study of green rust. M.Sc. thesis, Äspö Hard Rock Laboratory, Geological Institute, University of Copenhagen, Denmark.

Ciuk, E., 1970. Schemes of the Tertiary from the Polish Lowland area (in Polish with English summary). Kwartalnik Geologiczny, **14** (4): 754–771.

Ciuk, E., Pożaryska, K., 1982. On paleogeography of the Tertiary of the Polish Lowlands. Prace Muzeum Ziemi, **35**: 81–88.

Colombo, C., Palumbo, G., Di Iorio, E., Russo, F., Terribile, F., Jiang, Z., Liu, Q., 2016. Soil development in a Quaternary fluvio-lacustrine paleosol sequence in Southern Italy. Quaternary International, **418**: 195–207; https://doi.org/ 10.1016/j.quaint.2015.11.004

Cornell, R.M., Schwertmann, U., 2003. The Iron Oxides – Structure, Properties, Reactions, Occurrences and Uses, 2nd ed. Wiley-VCH Verlag, Weinheim.

Cuadros, J., Sánchez-Marañón, M., Mavris, C., Fiore, S., Bishop, J. L., Melgosa, M., 2020. Colour analysis and detection of Fe minerals in multi-mineral mixtures from acid-alteration environments. Applied Clay Science, **193**, 105677; https://doi.org/10.1016/j.clay.2020.105677

Duczmal-Czernikiewicz, A., 2010. Geochemistry and mineralogy of the Poznań Formation (Polish Lowlands). Adam Mickiewicz University Press, Poznań.

Duczmal-Czernikiewicz, A., 2013. Evidence of soils and palaeosols in the Poznań Formation (Neogene, Polish Lowlands). Geological Quarterly, **57** (2): 189–204; https://doi.org/10.7306/gq.1082

Dyar, M.D., Agresti, D.G., Schaefer, M.W., Grant, Ch.A., Sklute, E.C., 2006. Mössbauer Spectroscopy of Earth and Planetary Materials. Annual Review of Earth and Planetary Sciences, **34**: 83–125; https://doi.org/10.1146/annurev.earth.34.031405.125049

Dyjor, S., 1970. The Poznań series in West Poland (in Polish with English summary). Kwartalnik Geologiczny, **14** (4): 819–835.

Goldstein, J.I., Newbury, D.E., Michael, J.R., Ritchie, N.W., Scott, J.H.J., Joy, D.C., 2017. Scanning Electron Microscopy and X-ray Microanalysis. 4th edition. Springer, New York.

Górniak, K., Szydłak, T., Sikora, W.S., Gaweł, A., Bahranowski, K., Ratajczak T., 2001. Clay minerals in colourful rocks appearing over lignite deposits in Konin region (in Polish with English summary). Górnictwo Odkrywkowe, **43**: 129–139.

Górnicki, R., Błachowski, A., Ruebenbauer, K., 2007. Mössbauer Spectrometer MsAa-3. Nukleonika, **52** (suppl. 1): S7–S12.

Habashi, F., 2016. Pigments through the Ages. InterCeram, International Ceramic Review, **65**: 156–165; https://doi.org/10.1007/BF03401164

Hartemink, A.E., 2009. The depiction of soil profiles since the late 1700s. Catena, **79**: 113–127; https://doi.org/10.1016/j.catena.2009.06.002

Huang, J., Zhang, H., 2020. Redox reactions of iron and manganese oxides in complex systems. Frontiers of Environmental Science & Engineering, **14**, 76; https://doi.org/10.1007/s11783-020-1255-8

Jiang, Z., Liu, Q., Roberts, A.P., Dekkers, M. J., Barrón, V., Torrent, J., Li, S., 2022. The magnetic and colour reflectance properties of hematite: from Earth to Mars. Reviews of Geophysics, **60**, e2020RG000698; https://doi.org/10.1029/2020RG000698

Johnson, C.A., 2014. Observations and assessment of iron oxide nanoparticles in metal-polluted mine drainage within a steep redox gradient, and a comparison to synthetic analogs. Ph.D. thesis, Virginia Polytechnic Institute and State University.

Kasiński, J.R., Słodkowska, B., 2016. Factors controlling Cenozoic anthracogenesis in the Polish Lowlands. Geological Quarterly, **60** (4): 959–974; https://doi.org/10.7306/gq.1321

Kędzior, A., Widera, M., Zieliński, T., 2021. Ancient and modern anastomosing rivers: insights from sedimentological and geomorphological case studies of the Triassic, Neogene and Holocene of Poland. Geological Quarterly, **65**, 54; https://doi.org/10.7306/gq.1623

Kisch, H.J., 1990. Calibration of the anchizone: a critical comparison of illite 'crystallinity' scales used for definition. Journal of Metamorphic Geology, **8**: 31–46; https://doi.org/10.1111/j.1525-1314.1990.tb00455.x

Klęsk, J., 2023. Sulphur and its main minerals in the "Poznań Clays" (upper Neogene) – their influence on the sediment colour (in Polish with English summary). Przegląd Geologiczny, **71**: 249–254; https://doi.org/10.7306/2023.22

Klęsk, J., Błachowski, A., Diduszko, R., Kruszewski, Ł., Widera, M., 2022. Iron-bearing phases affecting the colour of upper Neogene clayey sediments from Dymaczewo Stare, west-central Poland. Geologos, **28**: 129–139; https://doi.org/0.2478/logos-2022-0010

Klęsk, J., Błachowski, A., Kruszewski, Ł., Michalska, D., Mrozek-Wysocka, M., Widera, M., 2023. Colours of the upper Neogene "Poznań Clays" in the light of sedimentological, mineralogical and nuclear methods. Geological Quarterly, **67**, 49; https://doi.org/10.7306/gq.1719

Kraus, M.J., 1999. Paleosols in clastic sedimentary rocks: their geologic applications. Earth-Science Reviews, **47**: 41–70; https://doi.org/10.1016/S0012-8252(99)00026-4

Kraus, M.J., Aslan, A., 1993. Eocene hydromorphic paleosols: significant for interpreting ancient floodplain processes. Journal of Sedimentary Petrology, **63**: 453–463; https://doi.org/10.1306/D4267B22-2B26-11D7-8648000102C1865D

Kraus, M.J., Riggins, S., 2007. Transient drying during the Paleocene–Eocene Thermal Maximum (PETM): Analysis of paleosols in the Bighorn basin, Wyoming. Palaeogeography, Palaeoclimatology, Palaeoecology, **245**: 444–461; https://doi.org/10.1016/j.palaeo.2006.09.011

Kruszewski, Ł., 2013. Supergene sulphate minerals from the burning coal mining dumps in the Upper Silesian Coal Basin, South Poland. International Journal of Coal Geology, **105**: 91–109; https://doi.org/10.1016/j.coal.2012.12.007

Kuhl, J., 1958. Clay-rich rocks associated with lignite in Konin and their potential uses (in Polish). Materiały Budowlane, **13**: 2–3.

Lempart-Drozd, M., Błachowski, A., Gumsley, A., Ciesielska, Z., 2022. Thermal decomposition of minnesotaite and dehydrogenation during Fe^{2+} oxidation, with implications for redox reactions in Banded Iron Formations. Chemical Geology, **601**, 120867; https://doi.org/10.1016/j.chemgeo.2022.120867

Maciaszek, P., Chomiak, L., Wachocki, R., Widera, M., 2019. The interpretive significance of ripple-derived sedimentary structures within the late Neogene fluvial succession, central Poland. Geologos, **25**: 1–13; https://doi.org/10.2478/logos-2019-0001

Maciaszek, P., Chomiak, L., Urbański, P., Widera, M., 2020. New insights into the genesis of the "Poznań Clays" – upper Neogene of Poland. Civil and Environmental Engineering Reports, **30**: 18–32; https://doi.org/10.2478/ceer-2020-0002

Makiel, M., Skiba, M., Kisiel., Maj-Szeliga, K., Błachowski, A., Szymański, W., Salata, D., 2022. Formation of iron oxyhydroxides as a result of glauconite weathering in soils of temperate climate. Geoderma, **416**, 115780; https://doi.org/10.1016/j.geoderma.2022.115780

Mameli, P., Mongelli, G., Oggiano, G., Dinelli, E., 2007. Geological, geochemical and mineralogical features of some bauxite deposits from Nurra (Western Sardinia, Italy): insights on conditions of formation and parental affinity. International Journal of Earth Sciences, **96**: 887–902; https://doi.org/10.1016/j.geoderma.2022.115780

Mancini, M., Weindorf, D.C., Carvalho Monteiro, M.E., Gomes de Faria, Á.J., dos Santos Teixeira, A.F., de Lima, W., Dias de Lima, F.R., Santos Branco Dijair, T., D'Auria Marques, F., Ribeiro, D., Godinho Silva, S.H., Chakraborty, S., Curi, N., 2020. From sensor data to Munsell colour system: Machine learning algorithm applied to tropical soil colour classification via Nix™ Pro sensor. Geoderma, **375**, 114471; https://doi.org/10.1016/j.geoderma.2020.114471

Mazur, J., 1959. Clays in the area of lignite deposits in the Konin region (in Polish). Węgiel Brunatny, **1**: 18–26.

McBride, E.F., 1974. Significance of color in red, green, purple, olive, brown, and gray beds of Difunta Group, northeastern Mexico. Journal of Sedimentary Petrology, **44**: 760–773; https://doi.org/10.1306/212F6B9A-2B24-11D7-8648000102C1865D

Mindat, 2022. Hudson Institute of Mineralogy, 1993–2022. https://www.mindat.org, retrieved 23.04.2026

Murad, E., 2010. Mössbauer spectroscopy of clays, soils and their mineral constituents. Clay Minerals, **45**: 413–430; https://doi.org/10.1180/claymin.2010.045.4.413

Murad, E., Cashion, J., 2004. Mössbauer Spectroscopy of Environmental Materials and their Industrial Utilization. Kluwer Academic Publishers, Norwell, Massachusetts.

Nemec, W., Porębski S., 1977. Weissliegendes sandstones: a transition from fluvial-aeolian to shallow-marine sedimentation (Permian of the Fore-Sudetic Monocline). 2. A study in significance of rock colouration. Annales Societatis Geologorum Poloniae, **47**: 513–544.

Nordstrom, D.K., 1982. Aqueous pyrite oxidation and the consequent formation of secondary iron minerals. Acid Sulfate Weathering, **10**: 37–56; https://doi.org/10.2136/sssaspecpub10.c3

Piwocki, M., Ziembińska-Tworzydło, M., 1997. Neogene of the Polish Lowlands – lithostratigraphy and pollen-spore zones. Geological Quarterly, **41** (1): 21–40.

Retallack, G.J., 2019. Soils of the Past. An Introduction to Paleopedology. 2nd edition. Wiley-Blackwell, Chichester.

Rietveld, H.M., 1969. A profile refinement method for nuclear and magnetic structures. Journal of Applied Crystallography, **2**: 65–71; https://doi.org/10.1107/S0021889869006558

Ristić, M., Krehula, S., Reissner, M., Musić, S., 2017. ^{57}Fe Mössbauer, XRD, FT-IR, FE SEM analyses of natural goethite, hematite and siderite. Croatica Chemica Acta, **90**: 499–507; https://doi.org/10.5562/cca3233

Schwertmann, U., 1993. Relations between iron oxides, soil colour, and soil formation. Soil Science Society of America, Special Publications, **31**: 51–69; https://doi.org/10.2136/sssaspecpub31.c4

Shepard, F.P., 1954. Nomenclature based on sand-silt-clay ratios. Journal of Sedimentary Research, **24**: 151–158; https://doi.org/10.1306/D4269774-2B26-11D7-8648000102C1865D

Soil Survey Staff, 1951. Soil survey manual. U.S. Department of Agriculture Handbook 18. U.S. Government Printing Office, Washington, D.C.

Środoń, J., Drits, V.A., McCarty, D.K., Hsieh, J.C.C., Eberl, D.D., 2001. Quantitative XRD analysis of clay-rich rocks from random preparations. Clays and Clay Minerals, **49**: 514–528.

Środoń, J., Szulc, J., Anczkiewicz, A., Jewuła, K., Banaś, M., Marynowski, L., 2014. Weathering, sedimentary and diagenetic controls of mineral and geochemical characteristics of the vertebrate-bearing. Silesian Keuper. Clay Minerals, **49**: 569–594; https://doi.org/10.1180/claymin.2014.049.4.07

TCMS, 2022. The Clay Minerals Society, Reynolds Cup Competition. https://www.clays.org/reynolds, retrieved 23.04.2026

Torrent, J., Schwertmann, U., Schulze, D.G., 1980. Iron oxide mineralogy of some soils of two river terrace sequences in Spain. Geoderma, **23**: 191–208; https://doi.org/10.1016/0016-7061(80)90002-6

Trąbska, J., 2015. Mikrostrukturalne przesłanki dla oceny pochodzenia i przetworzenia czerwonych surowców żelazistych („Ochr") na przykładzie wybranych stanowisk paleolitycznych (in Polish). University of Rzeszów, Poland.

Troć, M., Sadowska, A., 2006. The age of Poznań Formation in the area of Poznań (in Polish with English summary). Przegląd Geologiczny, **54**: 588–593.

Tucker, M.E., 2003. Sedimentary Rocks in the Field. John Wiley and Sons., Chichester, UK.

Tucker, M.E., 2011. Sedimentary Rocks in the Field: A Practical Guide. Wiley-Blackwell, Chichester, UK.

Turner, P., 1980. Continental red beds. Developments in Sedimentology, **29**.

Upreti, N., Srivastava, P., 2019. Role of latitudinal shift and climate change in evolution of red and yellow palaeosols of the Himalayas: implications for early Oligocene seasonality and Mid-Miocene enhanced precipitation. Sedimentology, **67**: 2189–2221; https://doi.org/10.1111/sed.12699

Urbański, P., Wachocki, R, Widera, M., 2025. Sedimentary record of the late Neogene avulsion process at the Tomisławice lignite opencast mine in central Poland – a new hypothesis. Acta Geologica Polonica, **75**, e55; https://doi.org/10.24425/agp.2025.155949

Valanciene, V., Siauciunas, R., Baltusnikaite, J., 2010. The influence of mineralogical composition on the colour of clay body. Journal of the European Ceramic Society, **30**: 1609–1617; https://doi.org/10.1016/j.jeurceramsoc.2010.01.017

Walker, A., 2018. Sorption Study of Se (-II) onto Illite, Bentonite, and Shale Under High Ionic Strength Conditions (Doctoral dissertation).

Wang, C., Ma, S., Lu, A., Zhou, J., 2005. The formation conditions of jarosite and its environmental significance. Acta Petrologica et Mineralogica, **24**: 607–611.

Warr, L.N., Mählmann, R.F., 2015. Recommendations for Kübler index standardization. Clay Minerals, **50**: 283–286; https://doi.org/10.1180/claymin.2015.050.3.02

Widera, M., 2007. Lithostratigraphy and palaeotectonics of the sub-Pleistocene Cenozoic of Wielkopolska. Adam Mickiewicz University Press, Poznań.

Widera, M., 2013. Sand- and mud-filled fluvial palaeochannels in the Wielkopolska Member of the Neogene Poznań Formation, central Poland. Annales Societatis Geologorum Poloniae, **83**: 19–28.

Widera, M., 2021. Geology of Polish lignite deposits (in Polish). Bogucki Wydaw. Naukowe, Poznań.

Widera, M., Szczurek, M., 2014. Anthropogenic mineral deposits in Wielkopolska lignite mines – current state of research (in Polish with English summary). Gospodarka Surowcami Mineralnymi, **30**: 21–38; https://doi.org/10.2478/gospo-2014-0001

Widera, M., Klęsk, J., 2025. Poznań Clays versus Poznań Formation in the upper Neogene of the Polish Lowlands: controversy about meaning, origin and age. Geological Quarterly, **69**, 17; https://doi.org/10.7306/gq.1719

Widera, M., Kowalska, E., Fortuna, M., 2017. A Miocene anastomosing river system in the area of Konin Lignite Mine, central Poland. Annales Societatis Geologorum Poloniae, **87**: 157–168; https://doi.org/10.14241/asgp.2017.012

Widera, M., Chomiak, L., Zieliński, T., 2019. Sedimentary facies, processes and paleochannel pattern of an anastomosing river system: an example from the Upper Neogene of Central Poland. Journal of Sedimentary Research, **89**: 487–507; https://doi.org/10.2110/jsr.2019.28

Widera, M., Bechtel, A., Chomiak, L., Maciaszek, P., Słodkowska, B., Wachocki, R., Worobiec, E., Worobiec, G., Zieliński, T., 2021a. Palaeoenvironmental reconstruction of the Konin Basin (central Poland) during lignite accumulation linked to the Mid-Miocene Climate Optimum. Palaeogeography, Palaeoclimatology, Palaeoecology, **568**, 110307; https://doi.org/10.1016/j.palaeo.2021.110307

Widera, M., Zieliński, T., Chomiak, L., Maciaszek, P., Wachocki, R., Bechtel, A., Słodkowska, B., Worobiec, E., Worobiec, G., 2021b. Tectonic-climatic interactions during changes of depositional environments in the Carpathian foreland: an example from the Neogene of central Poland. Acta Geologica Polonica, **71**: 519–542; https://doi.org/10.24425/agp.2020.134567

Widera, M., Chomiak, L., Wachocki, R., 2023. Distinct types of crevasse splays formed in the area of Middle Miocene mires, central Poland: insights from geological mapping and facies analysis. Sedimentary Geology, **443**, 106300; https://doi.org/10.1016/j.sedgeo.2022.106300

Wiewióra, A., Wyrwicki, R., 1974. Clay minerals in the mottled clay horizon of the Poznań series (in Polish with English summary). Kwartalnik Geologiczny, **18** (3): 615–635.

Wiewióra, A., Wyrwicki, R., 1976. Beidellite from the sediments of the Poznań series (in Polish with English summary). Kwartalnik Geologiczny, **20** (2): 331–341.

Wyrwicki, R., 1969. Gypsum in Pliocene sediments (in Polish with English summary). Przegląd Geologiczny, **17**: 488–494.

Wyrwicki, R., 1974. Clay sediments of the Poznań series as ceramic raw materials (in Polish with English summary). Biuletyn Instytutu Geologicznego, **280**: 107–215.

Wyrwicki, R., 1975. Mineral composition and economic value of variegated Poznań clays (Pliocene) (in Polish with English summary). Kwartalnik Geologiczny, **19** (3): 633–648.

Wyrwicki, R., Wiewióra, A., 1981. Clay minerals of the Upper Miocene sediments in Poland. Bulletin Polish Academy of Sciences, Earth Sciences, **29**: 67–71.

Zachos, J., Pagani, M., Sloan, L., Thomas, E., Billups, K., 2001. Trends, rhythms, and aberrations in global climate 65 Ma to present. Science, **292**: 686–693; https://doi.org/10.1126/science.1059412

Zatoń, M., Rakociński, M., Marynowski, L., 2008. Pyrite framboids as paleoenvironmental indicators. Przegląd Geologiczny, **56**: 158–164.

Zieliński, T., 2014. Sedymentologia. Osady rzek i jezior (in Polish). Wydaw. Naukowe UAM, Poznań.

Zieliński, T., Widera, M., 2020. Anastomosing-to-meandering transitional river in sedimentary record: a case study from the Neogene of central Poland. Sedimentary Geology, **404**, 105677; https://doi.org/10.1016/j.sedgeo.2020.105677